Low-lying 2^+ states generated by *pn*-quadrupole correlation and $N = 28$ shell quenching

Shuichiro Ebata[1] and Masaaki Kimura[2]
[1]*Meme Media Laboratory, Hokkaido University, Sapporo, 060-0813, Japan*
[2]*Department of Physics, Hokkaido University, Sapporo, 060-0810, Japan*
(Received 13 March 2014; revised manuscript received 12 November 2014; published 13 January 2015)

The quadrupole vibrational modes of neutron-rich $N = 28$ isotones (^{48}Ca, ^{46}Ar, ^{44}S, and ^{42}Si) are investigated by using the canonical-basis time-dependent Hartree–Fock–Bogoliubov theory with several choice of energy density functionals, including nuclear pairing correlation. It is found that the quenching of the $N = 28$ shell gap and the proton holes in the *sd* shell trigger quadrupole correlation and increase the collectivity of the low-lying 2^+ state in ^{46}Ar. It is also found that the pairing correlation plays an important role to increase the collectivity. We also demonstrate that the same mechanism to enhance the low-lying collectivity applies to other $N = 28$ isotones ^{44}S and ^{42}Si, and it generates a couple of low-lying 2^+ states which can be associated with the observed 2^+ states.

DOI: 10.1103/PhysRevC.91.014309 PACS number(s): 21.10.Pc, 21.10.Re, 21.60.Jz, 27.40.+z

I. INTRODUCTION

As represented by the pygmy dipole mode [1–4], there are novel excitation modes peculiar to unstable nuclei. In particular, the low-lying collective excitation modes are quite sensitive to the underlying shell structure and the pairing correlations, and hence the quenched shell gaps in unstable nuclei should generate unique collective modes.

One of the interesting examples is the $N = 28$ shell gap which is known to be quenched in the vicinity of ^{44}S and which has been given considerable experimental [5–21] and theoretical attention [22–32]. Since the the orbital angular momenta of $f_{7/2}$ and $p_{3/2}$ differ by two, the quench of the $N = 28$ shell gap will lead to the strong quadrupole correlation of neutrons. Furthermore, the protons in Si, S, and Ar isotopes occupy the middle of the *sd* shell, and hence, the quadrupole correlation should also exist in the proton side. Therefore, once the $N = 28$ shell gap is quenched, the strong quadrupole correlations among protons and neutrons will be ignited and lead to a novel variety of the excitation modes. Indeed, various exotic phenomena such as the shape transition in Si and S isotopes and the coexistence of various deformed states are theoretically suggested [30–32].

In this paper, we report the low-lying quadrupole excitation modes in ^{46}Ar, ^{44}S, and ^{42}Si generated by the strong quadrupole correlation between protons and neutrons. To access the low-lying quadrupole modes of these isotopes, we apply the canonical-basis time-dependent Hartree–Fock–Bogoliubov (Cb-TDHFB) theory [33] which has been successfully applied to the study of the dipole [33,34] and quadrupole [35] resonances of nuclei of wide mass range. The Cb-TDHFB can describe self-consistently the dynamical effects of pairing correlation which has a significant role in generating the low-lying quadrupole strength, as reported in Refs. [36–40].

This paper is organized as follows: In Sec. II, we present the Cb-TDHFB equations, the choice of energy density functional, and the method to evaluate the strength function of quadrupole modes and $B(E2)$. In Sec. III, the results of ^{48}Ca and ^{46}Ar obtained by using the Skyrme SkI3 parameter set are presented, and the enhancement of the low-lying quadrupole mode in ^{46}Ar is demonstrated. The interaction dependencies of the results are also discussed. Furthermore, the low-lying states of other $N = 28$ isotones (^{44}S, ^{42}Si) are also investigated. Finally, Sec. IV summarizes this work.

II. FORMULATION

In this section, we introduce the Cb-TDHFB equation briefly, choice of interaction, and the method to evaluate the quadrupole strength function and $B(E2)$.

A. Canonical-basis time-dependent Hartree–Fock–Bogoliubov equation

By assuming the diagonal form of the pairing functional, the Cb-TDHFB equations [33] are derived from the full TDHFB equation represented in the canonical basis $\{\phi_l(t),\phi_{\bar{l}}(t)\}$ which diagonalize a density matrix. The Cb-TDHFB equations describe the time evolution of the canonical pair $\{\phi_l(t),\phi_{\bar{l}}(t)\}$, and its occupation probability $\rho_l(t)$ and pair probability $\kappa_l(t)$,

$$\begin{aligned} i\frac{\partial}{\partial t}|\phi_l(t)\rangle &= [h(t) - \eta_l(t)]\,|\phi_l(t)\rangle, \\ i\frac{\partial}{\partial t}|\phi_{\bar{l}}(t)\rangle &= [h(t) - \eta_{\bar{l}}(t)]|\phi_{\bar{l}}(t)\rangle, \\ i\frac{d}{dt}\rho_l(t) &= \kappa_l(t)\,\Delta_l^*(t) - \kappa_l^*(t)\,\Delta_l(t), \\ i\frac{d}{dt}\kappa_l(t) &= [\eta_l(t) + \eta_{\bar{l}}(t)]\kappa_l(t) + \Delta_l(t)\,[2\rho_l(t) - 1], \end{aligned} \tag{1}$$

where $\eta_l(t) \equiv \langle\phi_l(t)|h(t)|\phi_l(t)\rangle$, and the $h(t)$ and $\Delta_l(t)$ are the single-particle Hamiltonian and the gap energy, respectively. The numerical calculation was performed in the three-dimensional Cartesian coordinate space representation. The canonical basis $\phi_l(\boldsymbol{r},\sigma;t) = \langle\boldsymbol{r},\sigma|\phi_l(t)\rangle$ with $\sigma = \pm 1/2$ is expressed in the space which is discretized in a square mesh of 1.0 fm inside of a sphere of radius 18 fm. We introduce the absorbing boundary condition (ABC) to eliminate unphysical modes by adding a complex potential $-i\xi(\boldsymbol{r})$ to the single-particle Hamiltonian $h(t)$ in accordance with Refs. [41,42].

Here $\xi(\boldsymbol{r})$ is given as

$$\xi(\boldsymbol{r}) = \begin{cases} 0 & (\text{for } 0 < r < R_0) \\ \xi_0 \frac{|\boldsymbol{r}|-R_0}{r_{\rm ABC}} & (\text{for } R_0 < r < R), \end{cases} \quad (2)$$

where $R = R_0 + r_{\rm ABC} = 18$ fm. We set the ABC effective range $r_{\rm ABC} = 6$ fm and the depth $\xi_0 = 3.75$ MeV.

B. Choice of energy density functional

We apply the Skyrme functionals to the particle-hole (ph) channel. Unless otherwise mentioned explicitly, we adopt the SkI3 parameter set [43] which, among the parameter sets we tested, most reasonably describes the proton and neutron single-particle levels in the vicinity of ^{48}Ca. It is experimentally known that the $N = 28$ shell gap is approximately 4.8 MeV [44] and the proton $s_{1/2}$ is a few hundreds of keV above $d_{3/2}$ [45,46]. To investigate the interaction dependence of the results, we also show the results obtained SkM* parameter set [47], that yields a smaller $N = 28$ shell gap and a different order of proton $s_{1/2}$ and $d_{3/2}$ shells.

We use a schematic pairing functional form that was employed in Ref. [33]. The pairing energy $E_{\rm pair}$ and gap parameter $\Delta_l(t)$ are written as

$$E_{\rm pair} \equiv -\sum_{\tau=n,p} G_0^\tau \sum_{k,l>0} f\left(\varepsilon_k^{\tau 0}\right) f\left(\varepsilon_l^{\tau 0}\right) \kappa_k^\tau(t) \kappa_l^{\tau *}(t), \quad (3)$$

where the cutoff function $f(\varepsilon)$ depends on the single-particle energy $\varepsilon_l^{\tau 0}$ in the ground state [33,34]. In this work, we tested several choices of the pairing strength G_0^τ, which will be explained in the next section.

C. Strength function and $B(E2)$

In order to induce quadrupole responses, we add a weak instantaneous external field $V_{\rm ext}(\boldsymbol{r},t) = \eta \hat{F}_K(\boldsymbol{r})\delta(t)$ to initial states of the time evolution. Here the quadrupole external field acting on proton, neutron, isoscalar (IS), and isovector (IV) channels are given as $\hat{F}_K \equiv (\frac{1\mp\tau_z}{2}, 1 \text{ or } \tau_z) \otimes (r^2 Y_{2K} + r^2 Y_{2-K})/\sqrt{2(1+\delta_{K0})}$. The amplitude of the external field is so chosen to be a small number $\eta = 1 \sim 3 \times 10^{-3}$ fm^{-2} to guarantee the linearity. The strength function $S(E;\hat{F}_K)$ in each channel is obtained through the Fourier transformation of the time-dependent expectation value $\mathcal{F}_K(t) \equiv \langle\Psi(t)|\hat{F}_K|\Psi(t)\rangle$:

$$\begin{aligned} S(E;\hat{F}_K) &\equiv \sum_n |\langle\Psi_n|\hat{F}_K|\Psi_0\rangle|^2 \delta(E_n - E) \\ &= \frac{-1}{\pi\eta} \mathrm{Im} \int_0^\infty \{\mathcal{F}_K(t) - \mathcal{F}_K(0)\} e^{i(E+i\Gamma/2)t} dt, \end{aligned} \quad (4)$$

where $|\Psi_0\rangle$ and $|\Psi_n\rangle$ are the ground and excited states, respectively, while $|\Psi(t)\rangle$ is a time-dependent many-body wave function described by Cb-TDHFB equations. Γ is a smoothing parameter set to 1 MeV. We also performed unperturbed calculations in which $h(t)$ in Eq. (1) is replaced with the static single-particle Hamiltonian $h(t=0)$ computed by using the ground-state density. By comparing the results obtained by the fully self-consistent and unperturbed calculations, we investigate the effects of the residual interaction on the collectivity of the low-lying states.

To analyze the peak structure, we fit the $S(E;\hat{F}_K)$ below 10 MeV by the sum of Lorentzians $\mathfrak{L}_k(E;\hat{F}_K)$:

$$\begin{aligned} S(E;\hat{F}_K) &\simeq \sum_k \mathfrak{L}_k(E;\hat{F}_K) \\ &\equiv \sum_k \frac{a_k^\tau (\Gamma/2)^2}{[E - E(2_k^+)]^2 + (\Gamma/2)^2}, \end{aligned} \quad (5)$$

where k is a label of 2^+ state and Γ corresponds to the smoothing parameter in Eq. (4). The reduced transition probabilities in the proton and neutron channels, which are denoted as $B_k(E2\uparrow)$ and $B_k(N2\uparrow)$, are evaluated by integrating $\mathfrak{L}_k(E;\hat{F}_K)$ for each state,

$$\begin{aligned} B_k(E2\uparrow \text{ or } N2\uparrow) &\equiv \sum_K \left| \langle 2_k^+ | \hat{Q}_{2K} \frac{1 \mp \tau_z}{2} |0^+\rangle \right|^2 \\ &\simeq 5 \int_0^\infty \mathfrak{L}_k(E;\hat{F}_{K=0}) dE. \end{aligned} \quad (6)$$

The approximation in bottom line of Eq. (6) is reasonable for spherical nuclei such as ^{48}Ca and ^{46}Ar but gets worse for deformed nuclei ^{44}S and ^{42}Si.

We mention spurious modes in the present calculations. In our scheme, spurious modes (pairing rotation, spatial rotation, etc.) come up at zero energy in principle [33]. By the accurate time evolution using the fourth-order expansion of Cb-TDHFB to conserve particle number, and by preparing the ground-state wave function with the expectation value of center of mass less than 10^{-12} fm. These spurious modes are greatly reduced and almost invisible.

III. RESULTS AND DISCUSSIONS

A. ^{48}Ca and ^{46}Ar

First, we examine the quadrupole responses of double-closed-shell nucleus ^{48}Ca which is spherical and has no superfluid phase. The calculated neutron pf-shell gap 5.0 MeV, the order of proton $s_{1/2}$ and $d_{3/2}$, and their energy gap 0.57 MeV are consistent with the experimental data in the vicinity of ^{48}Ca [44–46]. The strength functions in the IS and IV channels shown in Fig. 1(a) have two peaks at 3.9 and 8.7 MeV in addition to the IS giant quadrupole resonance (GQR) at 20 MeV and the IVGQR having a broad distribution around 30 MeV. The properties of these two peaks below 10 MeV become clear by comparing the results in the proton and neutron channels [Figs. 1(b) and 1(c)]. Their strengths in the neutron channel are much larger than those in the proton channel showing the dominance of neutron excitation and their energies approximately agree with the neutron shell gaps between $f_{7/2}$-$p_{3/2}$ (5.0 MeV) and $f_{7/2}$-$f_{5/2}$ (8.4 MeV). Now we focus on the lowest peak to examine how the residual interaction affects the low-lying quadrupole modes by comparing the unperturbed and fully self-consistent results. The lowest peak at 5.0 MeV ($f_{7/2} \rightarrow p_{3/2}$) in the unperturbed neutron channel is lowered by 1.1 MeV and its strength is increased by a factor of 2.5 in the fully self-consistent results,

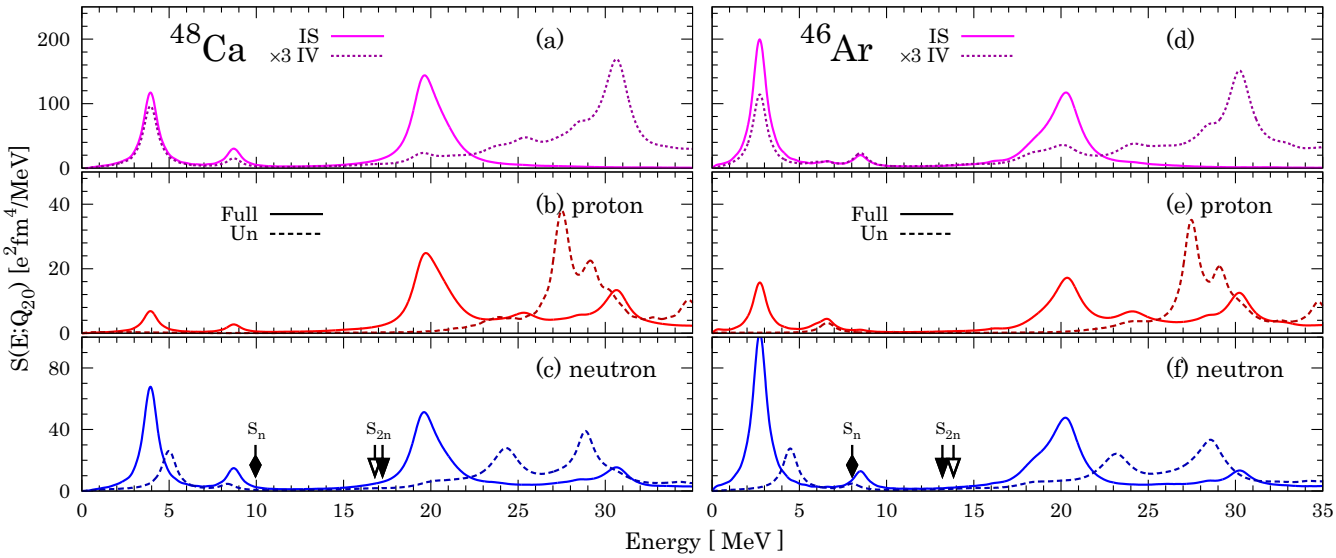

FIG. 1. (Color online) Strength functions of quadrupole vibrational modes of ^{48}Ca and ^{46}Ar. The strength functions in the IS (solid line) and IV (dotted line) channels are shown in panels (a) and (d), while those in the proton and neutron channels are shown in panels (b), (e) and (c), (f). The solid and dashed lines in the panels (b), (c), (e), and (f) compare the fully self-consistent and unperturbed results. The filled arrows show the experimental one- and two-neutron separation energies [50], while the open arrows show the calculated two-neutron separation energies.

as shown in Table I. The residual interaction between protons and neutrons induces a weak strength in the proton channel at the same energy where no strength exists in the unperturbed result, and hence this proton small peak cannot be attributed to the proton single-particle excitations. The evaluated first peak energy is $E(2^+) = 3.9$ MeV and $B(E2) = 52\ e^2$ fm$^4 \simeq 1.0$ W.U. (Weisskopf unit) listed in Table I reasonably agree with those of the observed 2^+ state, $E(2^+) = 3.83$ MeV and $B(E2) = 95 \pm 32\ e^2$ fm$^4 = 1.8 \pm 0.6$ in W.U. [48]. Although the observed and calculated $B(E2)$ strength are not as large as to be "collective", this result demonstrates that the residual interaction between protons and neutrons potentially induces proton collectivity even in the double-closed-shell nuclei. Naturally, we expect that this induction mechanism strongly depends on the size of the $N = 28$ shell gap and the shell ordering and energy gap of the proton *sd* shell, and we will see the proton collectivity is reinforced in neutron deficient $N = 28$ isotones in the following.

Now, we discuss the low-lying 2^+ states of ^{46}Ar. Here the proton pairing strength G_0^p is chosen so that the pairing gap reproduces the empirical value $\Delta^p = 2.7$ MeV evaluated by the three-points formula,[1] while that for neutrons is set to zero, which is consistent with the HFB calculations with Gogny force [25]. Other choice of pairing strength and the dependence of the results on the choice will be discussed in the next section. With this choice of G_0^p, the ground state of ^{46}Ar is spherical. If the proton pairing is switched off the ground state is oblately deformed ($\beta = -0.18$), which implies the weaker magicity of $N = 28$ in ^{46}Ar than ^{48}Ca. Indeed, the calculated $N = 28$ shell gap (see Table II) is slightly reduced in ^{46}Ar (4.5 MeV) compared with that in ^{48}Ca (5.0 MeV), which is consistent with observed gaps of ^{46}Ar (4.4 MeV) and ^{48}Ca (4.8 MeV) [44]. The unperturbed strengths in the proton and neutron channels in the Fig. 1(e) and 1(f) are quite similar to those of ^{48}Ca except for minor differences: (1) the reduction of the lowest peak energy in the neutron channel due to the quenching of the $N = 28$ shell gap, and (2) the small peak located around 6.6 MeV in the proton channel that is generated by the proton-hole states in the *sd* shell.

In the fully self-consistent results, strong peaks emerge around 2.7 MeV in all channels as shown in Figs. 1(d)–1(f). The neutron strength function looks similar to that of ^{48}Ca except for the very pronounced lowest peak. Similar to ^{48}Ca, the corresponding proton peak at the same energy is also induced due to the residual interaction. However, it is notable that energy of the lowest peak is considerably lowered and its strength is much more enhanced than ^{48}Ca, and their values are $B(E2\uparrow) = 114\ e^2$ fm^4 and $B(N2\uparrow) = 748\ e^2$ fm^4.

Experimentally, small and large values of $B(E2; 0_1^+ \to 2_1^+)$ at 1.55 MeV have been reported: in the Coulomb-excitation study $B(E2\uparrow) = 196 \pm 39$ $(218 \pm 31)\ e^2$ fm$^4 = 4.0 \pm 0.8$ (4.4 ± 0.6) W.U. [5,6], and in the lifetime

TABLE I. Peak position $E(2^+; \hat{F}_{K=0})$ [MeV] and the evaluated transition strengths $B(N2\uparrow)$ and $B(E2\uparrow)$ [e^2 fm^4] are also shown for ^{48}Ca and ^{46}Ar. The height a_k^τ [e^2 fm^4/MeV] of Lorentzian obtained by fitting the strength functions below 10 MeV [see Eqs. (5) and (6)].

	$E(2^+)$	$B(E2\uparrow)$	$B(N2\uparrow)$	$a_k^{\rm p}$	$a_k^{\rm n}$
^{48}Ca	3.9	52	510	6.9	67.8
	8.7	21	110	2.8	14.3
^{46}Ar	2.7	114	748	15.5	101.3
	6.6	36		4.7	
	8.5		94		12.2

[1] $\Delta^p(N,Z) = [2B(N,Z) - B(N,Z-1) - B(N,Z+1)]/2$, where $B(N,Z)$ is a binding energy.

TABLE II. Properties of the single-particle levels of ^{48}Ca and ^{46}Ar around the chemical potential. J, $\varepsilon_{\rm sp}$, and ρ_l denote their angular momenta, energies, and occupation probabilities, respectively. When ρ_l is an integer ("1" or "0"), the nucleus has no superfluid phase in neutron or proton. The single-particle states more than 7.5 MeV above the chemical potential are not shown, due to the cutoff energy in the pairing channel [33].

^{48}Ca						^{46}Ar					
Neutron			Proton			Neutron			Proton		
J	ε_l	ρ_l	J	ε_l	ρ_l	J	ε_l	ρ_l	J	ε_l	ρ_l
$f_{5/2}$	−1.42	0									
$p_{1/2}$	−3.00	0				$p_{1/2}$	−2.10	0			
$p_{3/2}$	−4.78	0				$p_{3/2}$	−3.61	0			
$f_{7/2}$	−9.78	1	$f_{7/2}$	−9.18	0	$f_{7/2}$	−8.09	1	$f_{7/2}$	−9.56	0.00
$d_{3/2}$	−19.05	1	$s_{1/2}$	−16.45	1	$d_{3/2}$	−17.39	1	$s_{1/2}$	−17.11	0.68
$s_{1/2}$	−19.13	1	$d_{3/2}$	−17.02	1	$s_{1/2}$	−17.58	1	$d_{3/2}$	−17.36	0.71
$d_{5/2}$	−25.28	1	$d_{5/2}$	−23.42	1	$d_{5/2}$	−23.62	1	$d_{5/2}$	−23.76	0.97

measurement $B(E2\uparrow) = 570^{+335}_{-160}\, e^2\,\mathrm{fm}^4 = 11.6^{+7.8}_{-3.3}$ W.U. [8]. In both experiments, the $E(2^+)$ is decreased and the $B(E2)$ is enhanced compared with ^{48}Ca, although they have large discrepancy [8,49].

In this section, we focus on the low-lying quadrupole mode of the nuclei which have a neutron magic number $N = 28$ and their shape are spherical, i.e., ^{48}Ca and ^{46}Ar. The hole state in the sd shell is a very important "seed" to generate a strong lowest 2^+ state and to induce the pn-quadrupole correlation which does not appear in the double-closed-shell nucleus. The keys that the mode to get a stronger collectivity in ^{46}Ar will be due to the proton hole states and the neutron pf-shell quenching, while working the pairing correlation. To understand the mechanism of the 2^+ state, we investigate the interaction dependencies in ph and pp(hh) channel, namely structure and correlation dependencies in the next section.

B. Interaction dependence of ^{46}Ar

To investigate how the enhancement of the low-lying strength depends on the underlying nuclear structure, we tested several different combinations of the energy density functional in ph and pp(hh) channels. In any cases we tested, the low-lying quadrupole collectivity in ^{46}Ar is much more enhanced than in ^{48}Ca, but its magnitude and distribution depend on the single-particle structure and pairing strength. To illustrate it, we discuss three cases, which are denoted ^{46}Ar$^{\rm I}$, ^{46}Ar$^{\rm II}$, and ^{46}Ar$^{\rm III}$ in the following.

The first case, ^{46}Ar$^{\rm I}$, is calculated by using SkM* in the ph channel instead of SkI3, and the pairing strengths are determined in the same manner as that explained in Sec. III A, i.e., the strength G_0^p of protons is so chosen to reproduce the empirical pairing gap, while that of the neutron has vanished. This choice of the energy functional yields the proton and neutron single-particle levels listed in Table III, where the $N = 28$ shell gap (3.31 MeV) is smaller than those of SkI3 and observations, and the order of proton $d_{3/2}$ and $s_{1/2}$ is reverted in contradiction to the observations. Figure 2 shows the strength functions of ^{46}Ar$^{\rm I}$ in proton [Fig. 2(a)] and neutron channels [Fig. 2(b)], which are obtained in the fully self-consistent (solid lines) and the unperturbed (thin chain lines) calculations. As clearly seen, the enhancement of the low-lying collectivity similar to the results shown in Fig. 1 is confirmed. However, there are several differences between the SkI3 and SkM* results: first, the low-lying peak is split into two, and second, the low-lying strength is increased. The origin of the splitting may be attributed to the proton excitation from $s_{1/2} \to d_{3/2}$. As already mentioned, SkM* yields different ordering of the proton sd shell, $d_{3/2}$ is 1.2 MeV above $s_{1/2}$ and, hence, the corresponding proton excitation can be seen as a small peak at 1.2 MeV in the unperturbed proton strength function. By switching on the residual interaction, the proton excitation couples to the neutron excitations and grows to the peak at

TABLE III. Same as Table II, but for ^{46}Ar$^{\rm I,II,III}$.

	^{46}Ar$^{\rm I}$ (with SkM*)				^{46}Ar$^{\rm II}$ (with $\Delta^n \neq 0$)				^{46}Ar$^{\rm III}$ (with weak $\frac{\Delta^n \neq 0}{\Delta^p \neq 0}$)					
	Neutron		Proton		Neutron		Proton		Neutron			Proton		
J	ε_l	ρ_l	ε_l	ρ_l	ε_l	ρ_l	ε_l	ρ_l	J	ε_l	ρ_l	J	ε_l	ρ_l
$p_{1/2}$	−3.06	0			−2.05	0.08			$p_{1/2}$	−2.07	0.04			
$p_{3/2}$	−4.95	0			−3.63	0.20			$p_{3/2}$	−3.61	0.11			
$f_{7/2}$	−8.26	1	−10.09	0.03	−8.02	0.89			$f_{7/2}$	−8.05	0.94			
$d_{3/2}$	−12.83	1	−15.36	0.61	−17.08	0.99	−16.89	0.69	$d_{3/2}$	−17.22	1.00	$s_{1/2}$	−17.11	0.69
$s_{1/2}$	−15.22	1	−16.57	0.78	−17.57	0.99	−17.07	0.71	$s_{1/2}$	−17.57	1.00	$d_{3/2}$	−17.12	0.69
$d_{5/2}$	−19.34	1	−21.81	0.97	−23.46	1.00	−23.39	0.97	$d_{5/2}$	−23.54	1.00	$d_{5/2}$	−23.58	0.98

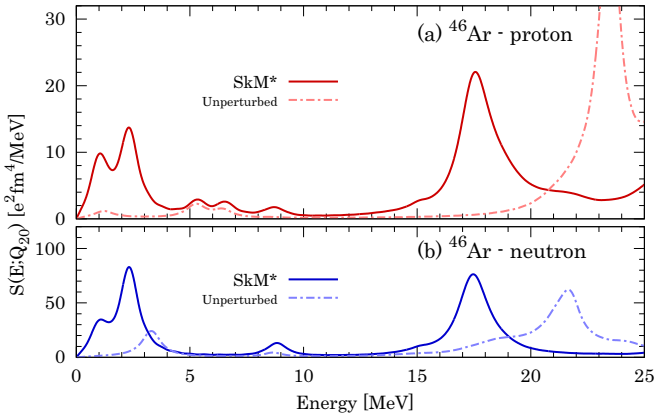

FIG. 2. (Color online) Strength functions in proton (red) and neutron (blue) channels for ^{46}Ar using SkM*. Fully self-consistent (thin solid line) and unperturbed (thin chain line) results are shown.

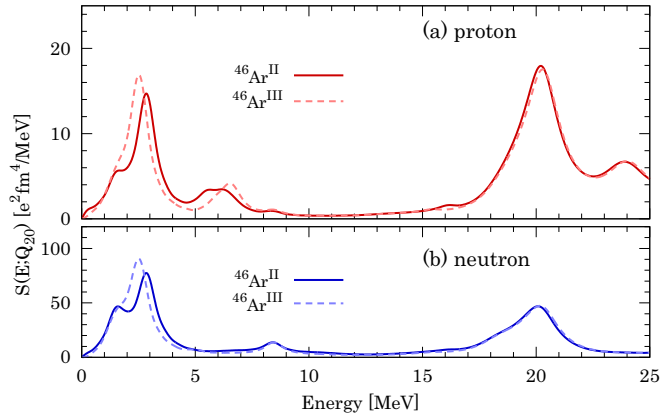

FIG. 3. (Color online) Strength functions in proton (red) and neutron (blue) channels for ^{46}Ar^{II} (solid line) and ^{46}Ar^{III} (dashed line), which are obtained by the fully self-consistent calculation.

1.1 MeV in the full calculation. On the other hand, the peak at 2.3 MeV has a nature similar to that of the SkI3 result, i.e., it is dominated by the neutron excitations across the $N = 28$ shell gap and the proton excitation is induced by the residual interaction. The relatively reduced $N = 28$ shell gap in SkM* dearly increases the amount of the strengths below 5 MeV [$S_{E2}^{5\mathrm{MeV}} \equiv 5\int_0^5 S(E;E2)dE$] from 109 e^2 fm^4 (SkI3) to 139 e^2 fm^4 (SkM*). The other visible differences are the small peaks around 7 MeV in the proton channel, which originate in the proton $d_{5/2} \rightarrow s_{1/2}$ and $d_{3/2}$ excitations and corresponds to the splitting of $s_{1/2}$ and $d_{3/2}$. The GQR is 17.5 MeV lower than that of SkI3, which has no drastic change.

It is well known that the pairing correlation has a significant role to form the low-lying quadrupole modes, as reported in Refs. [36–40]. Therefore, we now discuss two cases (^{46}Ar^{II} and ^{46}Ar^{III}) in order to investigate the pairing effects to low-lying 2^+ strength. The case ^{46}Ar^{II} is calculated by using SkI3 and the pairing strength G_0^τ are determined to reproduce empirical Δ^p and Δ^n simultaneously; in short, the pairing correlation in the neutron channel is turned on. In the case of ^{46}Ar^{III}, its pairing strengths are weakened to 85% of those of ^{46}Ar^{II}. The calculated single-particle levels in Table III show that the pairing in neutron channel changes the occupation probability of each orbit, but does not strongly affect the single-particle energies. The distributions of the strength functions shown in Fig. 3 are not drastically changed by switching on the neutron pairing, except for a shoulder around 1.5 MeV which appears due to the partial occupation of neutron p orbits. The major difference brought about by pairing correlation is the further enhancement of the low-lying collective mode. Here we check it by looking at the sum of the $E2$ strengths below 5 MeV; $S_{E2}^{5\mathrm{MeV}}$(^{46}Ar, ^{46}Ar^{II}, ^{46}Ar^{III}) = 109, 128, and 131 e^2 fm^4 are obtained. These results indicate that the pairing correlation tends to enhance the low-lying collectivity, but its magnitude is sensitive to the pairing strength.

Here, we also comment on the comparison between the present result and experimental data. The lifetime measurement [8] reports a value about three times larger than $B(E2) \sim 570\, e^2$ fm^4 than that reported by Coulomb-excitation experiments [5,6], $B(E2) \sim 196\,(218)\ e^2$ fm^4. In all cases we tested, the low-lying strengths are less than 200 e^2 fm^4, and hence supports the smaller value of $B(E2)$ reported by Coulomb excitation.

As a summary for this section, for all cases we tested, it is found that the low-lying collectivity is enhanced. It is also noted that the distribution and magnitude depend on the single-particle structure and pairing strength.

C. ^{42}Si and ^{44}S

The same mechanism also applies to other $N = 28$ isotones ^{44}S and ^{42}Si which are experimentally known to have deformed shape and low-lying 2^+ states [9–21]. In the present calculation, the pairing strengths in both channels are chosen to reproduce empirical gap energies. ^{44}S has a prolate shape ($\beta = 0.26$) with $\Delta^p = 2.37$ MeV and $\Delta^n = 1.12$ MeV, while ^{42}Si has an oblate shape ($\beta = -0.27$) with $\Delta^p = 2.70$ MeV and $\Delta^n = 1.04$ MeV. It is noted that the pattern of the deformed shape of the $N = 28$ isotone is consistent with other theoretical results [29–32,51,52]. Figure 4 shows their strength functions. Deformation of these nuclei splits the strength functions in the $K = 0$ and 2 modes and makes their strength distributions even more complicated than those in previous sections. However, we can still identify very-low-lying peaks which correspond to a couple of 2^+ states with enhanced collectivity. It is noted that, for example, three 2^+ states are observed in ^{44}S [17] and our results may be associated with some of them.

We also estimated 2^+ energies and $B(E2\uparrow)$ of ^{44}S and ^{42}Si by using Eqs. (5) and (6), although quantitative comparison with observation is not possible because of deformation of these nuclei. The first peak of ^{44}S at 1.0 MeV has a value of $B(E2\uparrow) = 103\ e^2$ fm^4 and that of ^{42}Si at 1.4 MeV has $B(E2\uparrow) = 47\ e^2$ fm^4. Similar to ^{46}Ar, the energies of 2^+ states have shifted to lower energy, and their strengths are significantly increased compared with ^{48}Ca. Indeed, in the experimental study of ^{44}S [11,12,15,16], a couple of low-lying 2^+ states and the enhancements of $B(E2)$ are reported; however, the observed $B(E2)$ is $310 \pm 90\ e^2$ fm^4 which is larger than our present result. This discrepancy could be

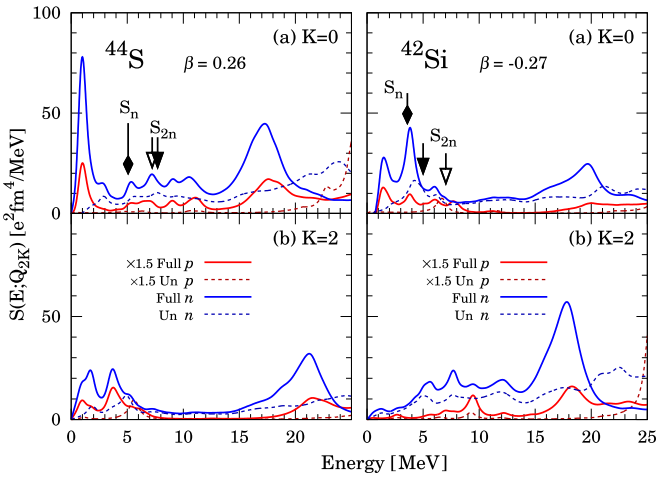

FIG. 4. (Color online) Strength functions in the proton and neutron channels for ^{44}S and ^{42}Si. $K = 0$ and 2 modes are shown in panels (a) and (b), respectively. The experimental separation energies S_n, S_{2n} are taken from Ref. [50].

attributed to the rotational mode caused by deformation of the ground band, as reported by experiments [9,21]. It is also noted the linear response method occasionally underestimates the observed $B(E2)$ as reported by Scamps and Lacroix [35] which could be another reason for the disagreement in ^{44}S and ^{42}Si.

IV. CONCLUSION

We investigated the low-lying quadrupole vibrational modes of $N = 28$ isotones (^{48}Ca, ^{46}Ar, ^{44}S, ^{42}Si) by using Cb-TDHFB theory. The proton low-lying 2^+ states of ^{48}Ca have neutron single-particle nature, which is found from the comparison of fully self-consistent and unperturbed results. Our calculation reproduces well not only the single-particle levels of the ground state but also the first 2^+ state and $B(E2)$ of ^{48}Ca. We discuss the mechanism of low-lying 2^+ excitation of other isotones based on the ^{48}Ca results. The 2^+ states of ^{46}Ar have a mechanism similar to ^{48}Ca, and the lowest peak indicates some collectivity which is triggered by proton hole states. Furthermore, we investigate the behavior of 2^+ strength functions under the change of interaction [ph, pp(hh) channel] for ^{46}Ar. From the investigation, we found that the peak position and the collectivity of the 2^+ states strongly depend on the relation among the neutron pf-shell gap, the level spacing in the proton sd shell, and the pairing strength. Our studies argue that the low-energy 2^+ state bringing a strong collectivity can be generated by these three pieces, also in a spherical system. Additionally, we found that the pairing correlation does not always enhance the collectivity of low-lying 2^+ states. In this study, we obtain prolate and oblate deformed ground states for ^{44}S and ^{42}Si. The multiple 2^+ states which appear in deformed nuclei can be applied the argued mechanism, although it could not explain the lowest 2^+ state of deformed nuclei. The mechanism of the 2^+ excited state can be induced near the region to violate ordinary magicity. We will apply the mechanism to other candidates in future work.

ACKNOWLEDGMENTS

We would like to thanks Professor T. Nakatsukasa for giving us the useful comments and advice. Computational resources were partially provided by the High Performance Computing System at the Research Center for Nuclear Physics, Osaka University.

[1] Y. Suzuki, K. Ikeda, and H. Sato, Prog. Theor. Phys. **83**, 180 (1990).
[2] A. Leistenschneider *et al.*, Phys. Rev. Lett. **86**, 5442 (2001).
[3] P. Adrich *et al.*, Phys. Rev. Lett. **95**, 132501 (2005).
[4] J. Gibelin *et al.*, Phys. Rev. Lett. **101**, 212503 (2008).
[5] H. Scheit *et al.*, Phys. Rev. Lett. **77**, 3967 (1996).
[6] A. Gade *et al.*, Phys. Rev. C **68**, 014302 (2003).
[7] L. A. Riley *et al.*, Phys. Rev. C **72**, 024311 (2005).
[8] D. Mengoni *et al.*, Phys. Rev. C **82**, 024308 (2010).
[9] T. Glasmacher *et al.*, Phys. Lett. B **395**, 163 (1997).
[10] F. Sarazin *et al.*, Phys. Rev. Lett. **84**, 5062 (2000).
[11] D. Sohler *et al.*, Phys. Rev. C **66**, 054302 (2002).
[12] S. Grevy *et al.*, Phys. Lett. B **594**, 252 (2004).
[13] J. Fridmann *et al.*, Phys. Rev. C **74**, 034313 (2006).
[14] B. Jurado *et al.*, Phys. Lett. B **649**, 43 (2007).
[15] M. Zielinska *et al.*, Phys. Rev. C **80**, 014317 (2009).
[16] C. Force *et al.*, Phys. Rev. Lett. **105**, 102501 (2010).
[17] D. Santiago-Gonzalez *et al.*, Phys. Rev. C **83**, 061305(R) (2011).
[18] J. Fridmann *et al.*, Nature (London) **435**, 922 (2005).
[19] B. Bastin *et al.*, Phys. Rev. Lett. **99**, 022503 (2007).
[20] L. Gaudefroy *et al.*, Phys. Rev. C **78**, 034307 (2008).
[21] S. Takeuchi *et al.*, Phys. Rev. Lett. **109**, 182501 (2012).
[22] J. Retamosa, E. Caurier, F. Nowacki, and A. Poves, Phys. Rev. C **55**, 1266 (1997).
[23] D. J. Dean, M. T. Ressell, M. Hjorth-Jensen, S. E. Koonin, K. Langanke, and A. P. Zuker, Phys. Rev. C **59**, 2474 (1999).
[24] G. A. Lalazissis, D. Vretenar, P. Ring, M. Stoitsov, and L. Robledo, Phys. Rev. C **60**, 014310 (1999).
[25] S. Péru, M. Girod, and J. F. Ferger, Eur. Phys. J. A **9**, 35 (2000).
[26] R. Rodríguez-Guzmán, J. L. Egido, and L. M. Robledo, Phys. Rev. C **65**, 024304 (2002).
[27] E. Caurier *et al.*, Rev. Mod. Phys. **77**, 427 (2005).
[28] L. Gaudefroy, Phys. Rev. C **81**, 064329 (2010).
[29] K. Kaneko, Y. Sun, T. Mizusaki, and M. Hasegawa, Phys. Rev. C **83**, 014320 (2011).
[30] Z. P. Li, J. M. Yao, D. Vretenar, T. Nikšić, H. Chen, and J. Meng, Phys. Rev. C **84**, 054304 (2011).
[31] T. R. Rodríguez and J. L. Egido, Phys. Rev. C **84**, 051307 (2011).
[32] M. Kimura, Y. Taniguchi, Y. Kanada-En'yo, H. Horiuchi, and K. Ikeda, Phys. Rev. C **87**, 011301 (2013).
[33] S. Ebata, T. Nakatsukasa, T. Inakura, K. Yoshida, Y. Hashimoto, and K. Yabana, Phys. Rev. C **82**, 034306 (2010).
[34] S. Ebata, T. Nakatsukasa, and T. Inakura, Phys. Rev. C **90**, 024303 (2014).

[35] G. Scamps and D. Lacroix, Phys. Rev. C **88**, 044310 (2013).
[36] M. Yamagami and Nguyen Van Giai, Phys. Rev. C **69**, 034301 (2004).
[37] K. Yoshida, M. Yamagami, and K. Matsuyanagi, Nucl. Phys. A **779**, 99 (2006).
[38] C. Losa, A. Pastore, T. Dossing, E. Vigezzi, and R. A. Broglia, Phys. Rev. C **81**, 064307 (2010).
[39] Y. Hashimoto, Eur. Phys. J. A **48**, 55 (2012).
[40] Y. Hashimoto, Phys. Rev. C **88**, 034307 (2013).
[41] T. Nakatsukasa and K. Yabana, J. Chem. Phys. **114**, 2550 (2001).
[42] T. Nakatsukasa and K. Yabana, Phys. Rev. C **71**, 024301 (2005).
[43] P.-G. Reinhard and H. Flocard, Nucl. Phys. A **584**, 467 (1995).
[44] L. Gaudefroy *et al.*, Phys. Rev. Lett. **97**, 092501 (2006).
[45] P. Doll, G. J. Wagner, K. T. Knöpfle, and G. Mairle, Nucl. Phys. A **263**, 210 (1976).
[46] S. M. Banks *et al.*, Nucl. Phys. A **437**, 381 (1985).
[47] J. Bartel, P. Quentin, M. Brack, C. Guet, and H. Håkansson, Nucl. Phys. A **386**, 79 (1982).
[48] S. Raman, C. W. Nestor, Jr., and P. Tikkanen, At. Data Nucl. Data Tables **78**, 1 (2001).
[49] R. Winkler *et al.*, Phys. Rev. Lett. **108**, 182501 (2012).
[50] M. Wang *et al.*, Chin. Phys. C **36**, 1603 (2012).
[51] P.-G. Reinhard, D. J. Dean, W. Nazarewicz, J. Dobaczewski, J. A. Maruhn, and M. R. Strayer, Phys. Rev. C **60**, 014316 (1999).
[52] Y. Utsuno, T. Otsuka, B. A. Brown, M. Honma, T. Mizusaki, and N. Shimizu, Phys. Rev. C **86**, 051301(R) (2012).